Journal of Petroleum Science and Technology 14(1): 41, 2024, Pages 16-30
DOI:10.22078/jpst.2024.5044.1860

Journal of Petroleum Science and Technology

Research Paper

https://jpst.ripi.ir/

Fracture Characterization and Prediction in a Volcanic Reservoir: A Case Study of the Permian Jiamuhe Formation in the Jinlong 2 Oil Field, Junggar Basin, China

Hui He[1], Chang Liu[1],*, Lin Xie[2], Chuixian Kong[3], Jianhong He[2], Xianming Li[2] and Pengshan Ma[1]

1. Research Institute of Petroleum Exploration and Development of PetroChina, Beijing, China

2. PetroChina Qinghai Oilfield Company, Dunhuang, Gansu, China

3. PetroChina Xinjiang Oilfield Company, Karamay, Xinjiang, China

Abstract

Fractures are the main flow channels for oil and gas in the Permian Jiamuhe Formation volcanic reservoir in the Jinlong 2 Oilfield at the northwestern margin of the Junggar Basin. Moreover, according to core, thin section, and image logging data analyses, the fractures in this area are dominantly semifilled or unfilled high-angle fractures, followed by semifilled low-angle oblique fractures and vertical fractures. Furthermore, the image logging results show that the fractures are oriented nearly east-west, approximately parallel to the direction of the present-day maximum principal in situ stress, and they have good flow effectiveness. In addition, the development of volcanic reservoir fractures is mainly affected by structure and lithology. Moreover, the fractures are primarily distributed in strips along the faults. The closer to the fault, the greater the structural curvature and the more developed the fractures. In addition, the fractures of intermediate–acid volcanic lava and pyroclastic lava are well-developed in the study area. Additionally, the fracture development characteristics of a single well are determined by calculating the fracture density, fracture dip angle, and fracture porosity. Ultimately, combined with the prestack seismic prediction method, i.e., amplitude versus azimuth (AVAZ), the attenuation initial frequency attribute is selected to predict the fracture distribution characteristics of the Jiamuhe Formation volcanic reservoir.

Keywords: Junggar Basin; Permian; Volcanic Reservoir; Fracture; Prestack Seismic Prediction.

Introduction

With the development of the global petroleum industry, volcanic oil and gas reservoirs have gradually become an important field of petroleum exploration and development. However, volcanic reservoirs are generally characterized by deep burial, complex structure, rapidly changing spatial variation of lithology and lithofacies, and strong heterogeneity, challenging reservoir description and prediction [1-10]. Moreover, the existing volcanic reservoir exploration and development practices have demonstrated that the degree of fracture development is an important factor in controlling oil and gas migration and reservoir enrichment and is favorable for efficient reservoir development. The fractures provide effective fluid flow channels, improve the oil and gas flow capacity, increase reservoir space, and enhance the drainage capacity and area [9, 11-22]. Therefore, describing volcanic reservoir fracture characteristics, analyzing the main controlling factors of fracture development, and predicting fracture distribution become essential to volcanic reservoir prediction, which is significant for effective exploration and development [5, 17, 23-28]. Moreover, the Jinlong 2 Oilfield in Xinjiang is located in the southern part of Zone 5 in the Karamay Oilfield, on the eastern slope of the Zhongguai Uplift at the northwestern margin of the Junggar Basin, where the Permian strata is one of the main oil systems. In 2012, high-yield commercial oil and gas flow was discovered in Well JIN201 in the Permian Jiamuhe Formation, which served as the prelude to exploring and developing a deep volcanic reservoir in this area.

The widespread fractures in the Jinlong 2 Oilfield volcanic rocks result from multiphase tectonic movements, and the fracture description of the Jiamuhe Formation volcanic reservoir has been complex. In addition, this study uses core observations, Formation Microscanner image (FMI) logging [3, 14, 29-33], and scanning electron microscopy data to identify the

**Corresponding author:* Chang Liu, *Research Institute of Petroleum Exploration and Development of PetroChina, Beijing, China*
E-mail addresses: liuchang1987@petrochina.com.cn
Received 2023-02-25, Received in revised form 2024-03-25, Accepted 2024-07-03, Available online 2024-10-21

fracture characteristics of the volcanic reservoir, summarize the fracture development behavior, and predict the fracture density and orientation through prestack seismic inversion. The study results provide a geological basis for the efficient development of the Jiamuhe Formation volcanic reservoir.

Geological Settings

The Jinlong 2 Block of the Jinlong Oilfield is located in the Karamay Oilfield (Fig. 1). The Permian Jiamuhe Formation (P1j) is the primary oil-bearing layer of the volcanic reservoir. It is deeply seated with an average depth of 4000 m (Fig. 2). Moreover, according to core observations and thin section identification, the lithology of the volcanic reservoir in the study area can be divided into three categories: volcanic lava, pyroclastic lava, and pyroclastic rocks. Subdivided further by composition, the volcanic lava includes basic basalt and amygdaloid basalt, intermediate–basic basaltic andesite, intermediate andesite, intermediate–acid dacite, acid rhyolite, vesicular rhyolite, and spheroidal rhyolite; pyroclastic lava includes basic basaltic (welded) breccia and intermediate andesitic (welded) breccia lavas; and pyroclastic rocks include intermediate andesitic agglomerate and andesitic breccia, intermediate–acid dacite tuff, and acid rhyolitic crystal tuff. Eight lithologies in three categories have been identified in the Jiamuhe Formation (Table 1), of which the favorable reservoir lithologies are andesitic volcanic breccia, volcanic breccia lava, andesite, and rhyolite. Volcanic explosive and eruptive facies are the main lithofacies units. The volcanic reservoir in the study area has low porosity (7.9%–20.4%; avg. 12.3%) and low to ultra-low permeability [(0.01–752) × 10^{-3} μm^2; avg. 0.69 × 10^{-3} μm^2]. Thin section observations indicate that the reservoir space comprises amygdaloid dissolved pores, vesicle and matrix pores, intraphenocryst pores, and microfractures. Moreover, according to mercury intrusion porosimetry experiments, the Jiamuhe Formation volcanic reservoir contains mainly micro–fine throats, with a maximum pore throat radii of 0.3 – 4.1 μm and dominant pore throat radii of 20–0.5 μm and moderately to poorly sorted, with displacement pressures of less than 0.03 MPa generally. In addition, such throats are found mainly in favorable reservoirs dominated by vesicles, amygdaloid andesite, andesitic volcanic breccia lava, and volcanic breccia. Fractures are widely developed in the reservoir, serving as the main flow channels of oil and gas in the study area.

Materials and Methods

Characteristics and Controlling Factors

Fracture Characteristics

Based on the core observations, image logging data, and thin sections, the natural fractures in the Jiamuhe Formation of the Jinlong 2 Oilfield can be divided into diagenetic and structural fractures according to their genesis. Diagenetic fractures can be subdivided into condensing shrinkage, breccia intergranular, interlayer, and dissolved fractures.

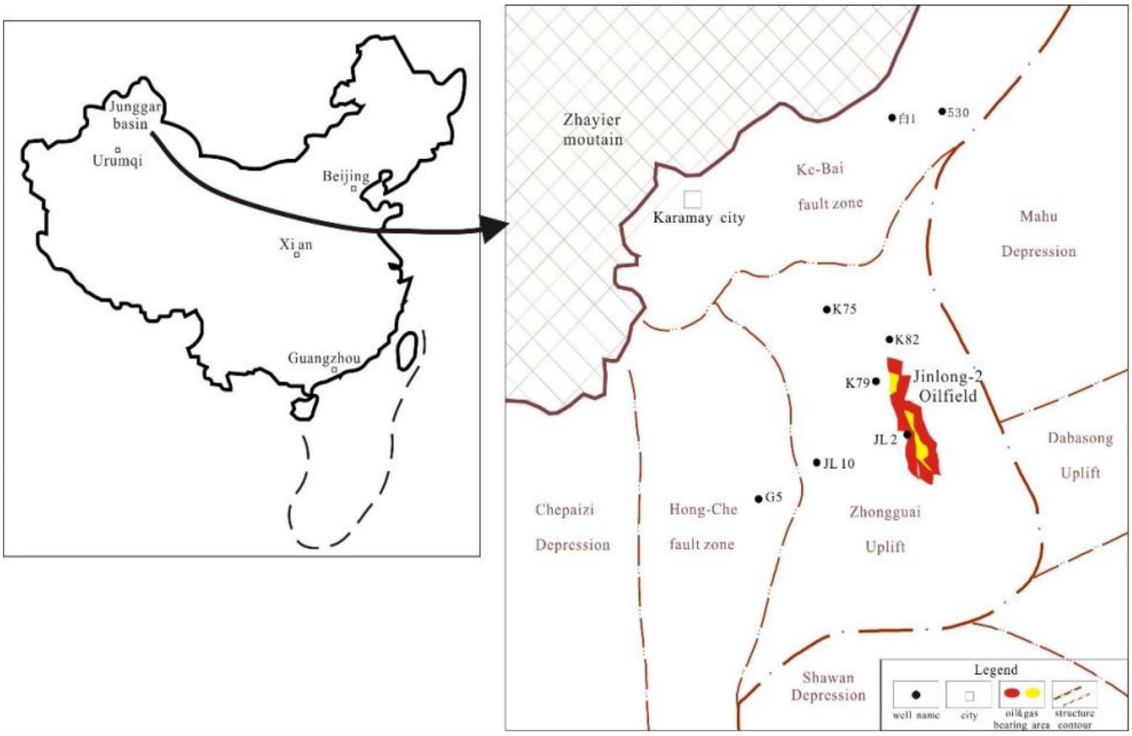

Fig. 1 Location of the Jinlong 2 Oilfield

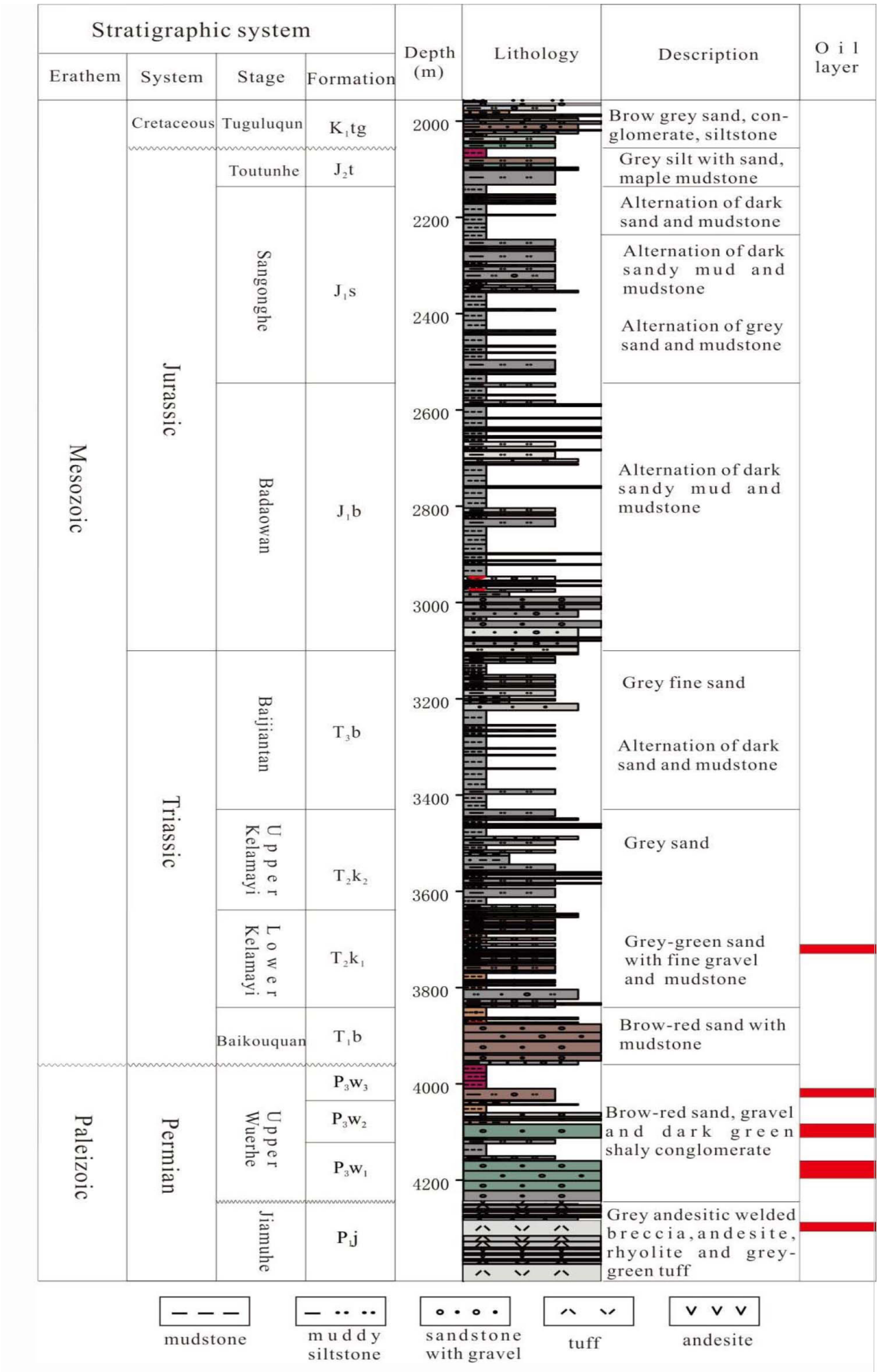

Fig. 2 The stratigraphic sequence of Jinlong 2 oilfield.

Table 1 Lithologic features and reservoir space types in the volcanic reservoir of the Jiamuhe Formation, Jinlong 2 Oilfield

Rock types		Colors	Textures	Structures	Typical wells	Reservoir space types	Core photo
Volcanic lava	Basalt	Dark gray, gray-brown	Interstitial	Massive, amygdaloid	JIN201	Amygdaloid pores, microfractures	
	Andesite	Gray-green, green-gray	Hyalopilitic	Amygdaloid, vesicle, massive	JIN204, JIN208	Vesicles, amygdaloid pores, microfractures	
	Rhyolite	Gray, light pink	Felsophyric–microgranular	Rhyolitic structure	JIN204, JIN213	Vesicles and matrix-dissolved pores	
Pyroclastic lava	Basaltic breccia lava	Dark gray, gray brown	Welded breccia	Amygdaloid	JIN201	Amygdaloid pores, microfractures	
	Andesitic breccia lava	Gray-green, green-gray	Welded breccia	Amygdaloid, vesicle, massive	JIN204, JIN208, JIN213	Vesicles, amygdaloid pores, microfractures	
Pyroclastic rocks	Andesitic volcanic breccia	Gray, gray brown	Tuffaceous breccia	Massive	JIN201, JIN214	Vesicles, matrix pores, microfractures	
	Dacitic tuff	Gray-brown, gray-green, gray	Lithic, crystal, breccia, tuffaceous	Massive	JIN204, JIN208 JL2	matrix dissolved pores, intracrystalline pores, microfractures	
	Rhyolitic crystalline tuff	Gray, light purplish red	Lithic, crystal	Rhyolitic and massive	JL2	Matrix-dissolved pores, intracrystalline pores, microfractures	

The fractures can also be divided into four types according to the dip angle: horizontal fractures (dip angle ≤ 15°), low-angle fractures (15° < dip angle ≤ 45°), high-angle fractures (45° < dip angle ≤ 75°), and vertical fractures (75° < dip angle ≤ 90°) (Table 2). Furthermore, horizontal fractures often develop in basalts, low to high Angle fractures can be seen in basaltic breccia lavas, and high Angle vertical fractures are common in Andesitic breccia lavas. Based on the cores and FMI data analysis (Fig. 3), the fractures in the study area are dominantly high-angle and vertical structural fractures, and the distribution range of fracture angles encompasses 6.3% for horizontal fractures, 8.6% for low-angle fractures, 42.6% for high-angle fractures, and 42.5% for vertical fractures.

Table 2 Types and characteristics of fractures in volcanic reservoirs of the Jiamuhe Formation in Jinlong 2 Oilfield

Item	Fracture type		Characteristic	Item	Fracture type	Characteristic
Genesis	Diagenetic fractures	Condensing shrinkage fractures	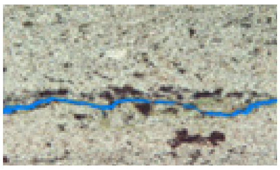 Sedimentary tuff	Occurrence	Horizontal fractures (dip angle ≤15°)	 Basalt
		Breccia intergranular fractures	 Volcanicbreccia		Low-angle fractures (15°< dip angle ≤ 45°)	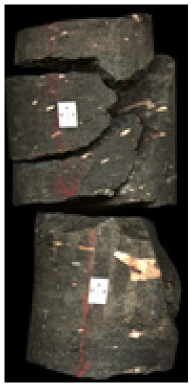 Basaltic breccia lava
		Interlayer fractures	 Andesite		High-angle fractures (45° < dip angle ≤ 75°)	
		Dissolved fractures	 Full-filled fractures in the andesite		Vertical fractures (75° < dip angle ≤ 90°)	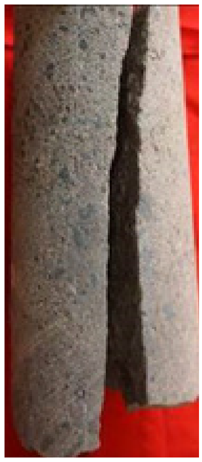 Andesitic breccia lava
	Structural fractures		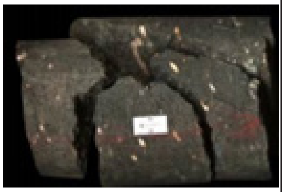 Basaltic breccia lava			
	Induced fractures		Fractures induced by drilling or downhole operations, not natural fractures; mostly arranged in echelon symmetry in FMI images			

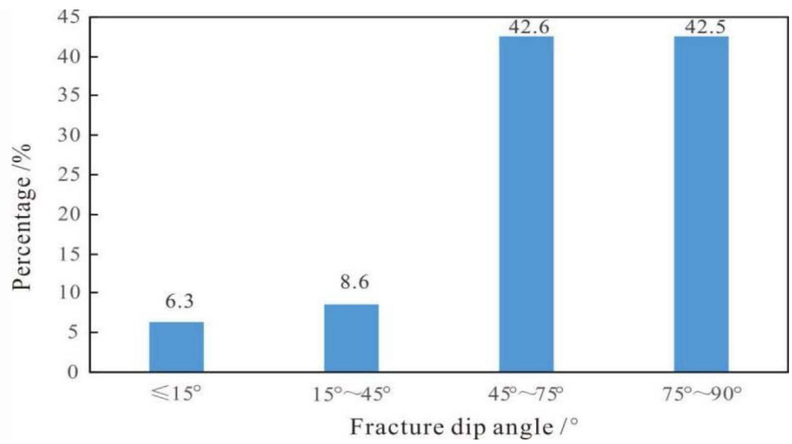

Fig. 3 Fracture dip angle distribution by core observation (6.3% for horizontal fractures, 8.6% for low-angle fractures, 42.6% for high-angle fractures, and 42.5% for vertical fractures, high-angle fractures are relatively developed)

Table 1 The results of N_2 adsorption-desorption analysis.

Catalyst	S BET (m^2/g)	S external (m^2/g)	V total (cm^3/g)	V micropore (cm^3/g)	V mesopore (cm^3/g)	D (nm)	HF[a]
Z-40	324	110	0.191	0.065	0.126	2.358	0.115
Z-120	374	215	0.287	0.086	0.201	3.069	0.172
Z-200	364	200	0.241	0.069	0.172	2.648	0.157
Z-Ce	355	205	0.265	0.083	0.182	2.985	0.181
Z-La	337	210	0.272	0.081	0.191	3.228	0.185

[a] HF = hierarchical factor = $(V_{micro}/V_{total})(S_{ext}/S_{BET})$

Ammonia-temperature Programmed Desorption Analysis

The results of the temperature-programmed desorption analysis for the synthesized zeolite samples are reported in Fig. 7 and Table 2. As seen in Fig. 7, the ammonia desorption profiles for all samples have desorption peaks in three regions: low temperature, medium temperature, and high temperature. These indicate three weak, medium, and strong acid site types for all zeolite samples, respectively. The reason for drastic changes in the amount of acidity for three synthesized zeolites (Z-40, Z-120, Z-200) can be the Si/Al ratio or, more specifically, the number of aluminum, according to which the amount of acidity and strength of acidity will also change [12, 27]. It is said that the smaller the number of aluminum in the zeolite unit cell, the more acid strength increases due to the isolation of aluminum atoms in the zeolite. The amount of total acidity and weak acidity in Z-Ce and Z-La samples has increased compared to their primary zeolite (Z-120) due to the RE compounds, possessing Lewis acidity properties, due to the presence of valence electrons and empty f orbitals in RE elements. Also, the amount of medium acidic sites has increased in them. The increase in medium acid sites is due to the interactions between metal species and inherent acid sites in ZSM-5 zeolite [3, 21].

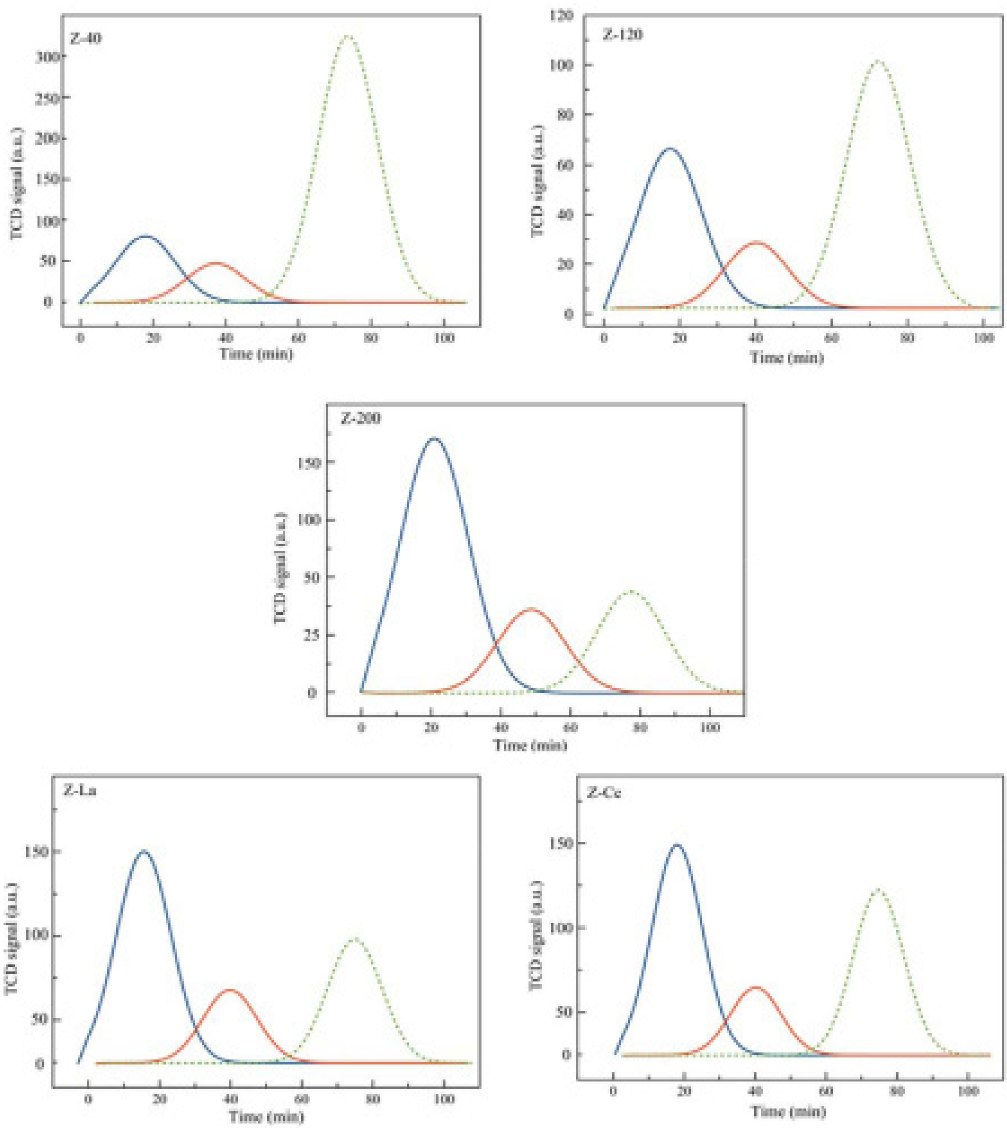

Fig. 7 NH_3-TPD profiles of prepared zeolite samples.

The whole core in situ stress analyses and FMI logging interpretations indicate that fractures in the Jiamuhe Formation are oriented nearly E–W (120° ± 5°), while the nearly S–N fractures are rare (Fig.4). The fracture dip direction interpreted by the core (black arrow) is basically consistent with the fracture dip direction interpreted by the imaging logging. The fractures are unfilled or semi-filled and rarely fully filled, usually with calcite, indicating that most of the fractures in volcanic reservoirs of the Jiamuhe Formation are effective oil and gas reservoirs (Table 2). Core observations and thin sections reveal traces of asphalt in half-filled or unfilled fractures, which function as oil and gas migration channels and occasionally for storage and seepage (Fig. 5). The FMI logging interpretation indicates that the fractures have dip angles mainly in the 20°–90° range, with an average of 65°, and high-angle fractures (dip angle > 45°) or vertical fractures are dominant (Table 3). The high-angle fractures are mainly structural shear fractures with flat fracture surfaces. The low-angle oblique fractures result from shear and tension and are mostly filled or semi-filled. According to previous studies [25], a fracture is effective when the angle between the orientation and this maximum principal stress direction is less than 30°. Moreover, the interpretations of core in situ stresses and single-well FMI logging results show that the orientations of the fracture in the study area are consistent with the maximum principal stress, and the natural fractures are effectively preserved. Therefore, high-angle or vertical fractures are adequate for developing volcanic reservoirs.

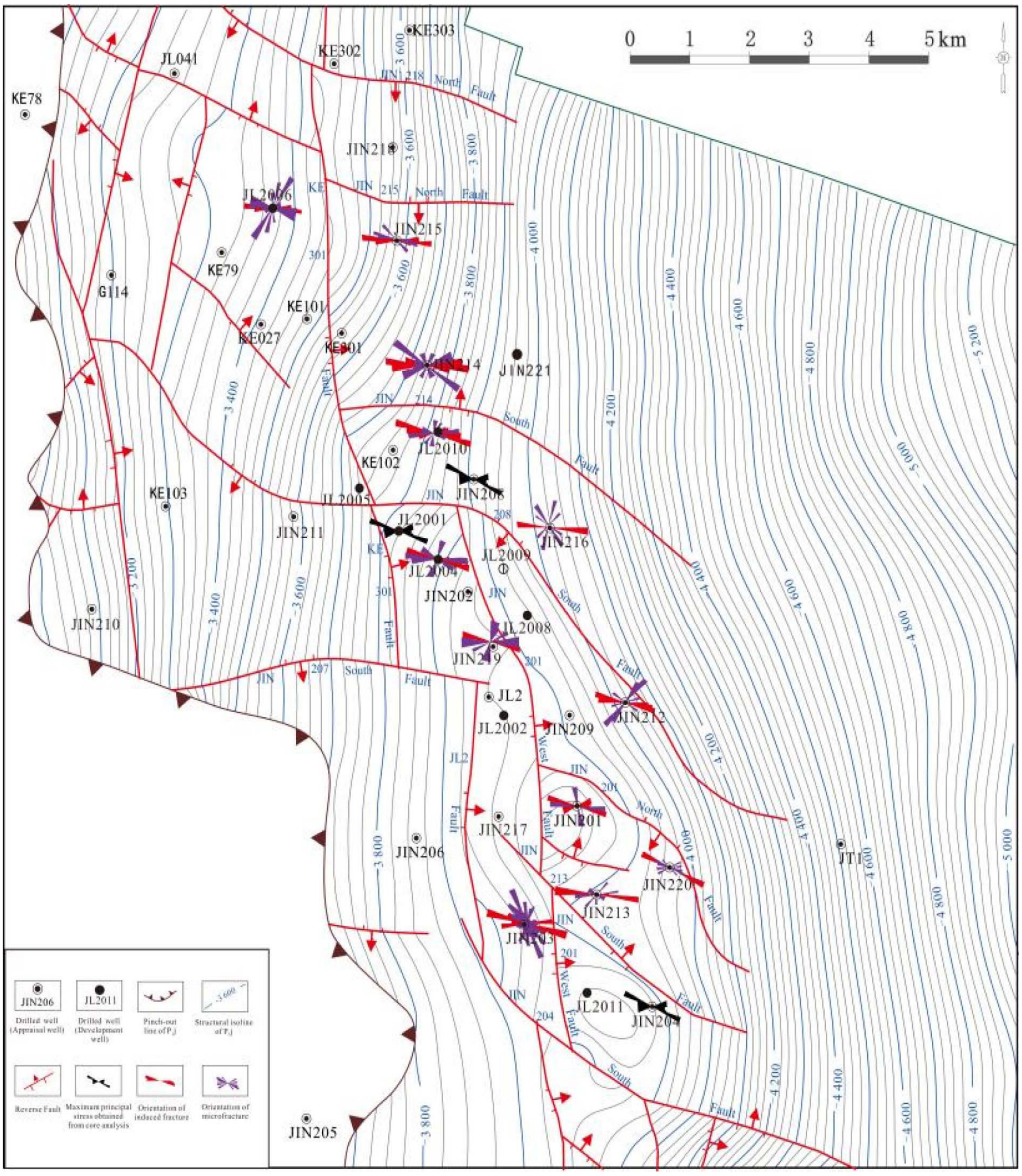

Fig. 4 Jiamuhe Formation (P1j) fracture orientation interpretation results in the Jinlong 2 Oilfield

a. JIN204, 4287.29 m, welded tuff, elongated siliceous semi-filled vesicles locally; asphalt observed in pores and microfractures.

b. JIN201, 4168.55 m, andesitic volcanic breccia, microfractures, chlorite, zeolite, and silicon; asphalt observed in microfractures

Fig. 5 The thin section of typical microfracture in the different volcanic rocks of Jiamuhe Formation (P1j)

Table 3 Formation microresistivity image (FMI) logging interpretation of fractures in Jiamuhe Formation (P1j) volcanic reservoir

well	Fracture density (fractures/m)	Fracture lenth (m)	Fracture with (mm)	Fracture porosity (%)	Fracture dip angle (°)	Fracture dip angle distribution
JIN213	2. 22～4. 54 / 3. 02	0. 55～3. 18 / 1. 71	0. 02～0. 05 / 0. 04	0. 01～0. 13 / 0. 07	20～70 / 56	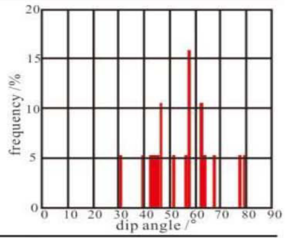
JIN201	0. 2～4. 67 / 1. 87	0. 43～4. 47 / 2. 26	0. 012～0. 1 / 0. 06	0. 01～0. 03 / 0. 01	20～60 / 45	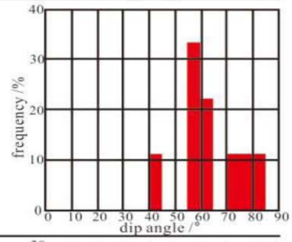
JL2004	0. 14～6. 93 / 2. 36	0.12～4. 47 / 1. 48	0. 02～0. 2 / 0. 09	0. 01～0. 41 / 0. 15	50～90 / 65	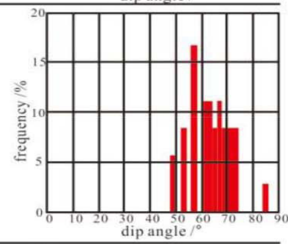
JL2010	0. 89～2. 62 / 1. 47	0. 84～1. 68 / 1. 47	0. 008～0. 017 / 0. 01	0. 008～0. 025 / 0. 02	40～85 / 65	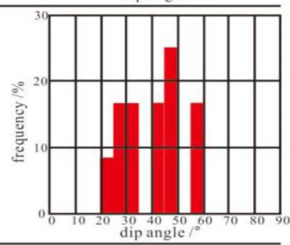
JIN215	0. 02～6. 09 / 2. 3	0. 49～2. 59 / 1. 51	0. 036～0. 186 / 0. 09	0. 018～0. 227 / 0. 13	30～80 / 58	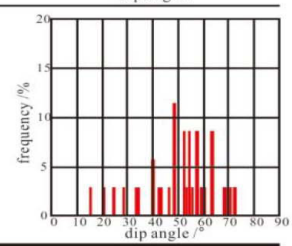

Note: Range of value / Average value

Controlling Factors

The structure and lithology are the main factors controlling fracture development in volcanic reservoirs [34-44]. The northwestern margin of the Junggar Basin experienced multiple phases of tectonic movement, such as the Hercynian, Indosinian, and Yanshanian orogenies. Moreover, the Permian Jiamuhe Formation volcanic complex was mainly controlled by the Hercynian and Indosinian movements, resulting in a nappe overthrusting along the detachment fault plane with a large fault throw from the slope in the east to the Carboniferous paleo uplift in the ancient mountains in the west. The study area contains two groups of reverse faults (NW–SE and nearly E–W), which controlled the formation of grouped structural fractures in the volcanic complex, thus increasing the complex fracture system in the Jinlong 2 Oilfield. In addition, the NW–SE reverse fault was formed under the nearly east-west compressive stress generated by the subduction of the western Junggar Ocean to the Kazakhstan Plate in the Middle-Late Carboniferous to Early Permian during the Hercynian movement. The fractures formed in this period are mainly NNE- and NNW-trending, tensional oblique fractures, mostly filled in the late stage and rarely at a high angle. In the Middle-Late Permian (from the late Hercynian to the early Indosinian), the collision compression and thrust gradually intensified, and the nappe continued to develop. Moreover, affected by the compressive stress, a nearly east-west, strike-slip reverse fault began to grow in the area. It intersected with the preexisting NW–SE reverse fault, cutting the study area into multiple fault blocks (Fig. 4). Affected by the nearly E–W strike-slip fault, tensile-shear fractures formed in this period, which are mostly high-angle fractures with good opening, trending NE and almost E–W, with large longitudinal cutting depth (length). In addition, the volcanic rocks that formed in the study area were subjected to two phases of strong compressive faulting, resulting in numerous structural fractures, significantly improving the permeability and reservoir capacity of the volcanic rocks. Generally, the bedding planes are bent and deformed when the strata are compressed by tectonic stress. Here, the relationship between deformation and tectonic curvature can be used to predict the fracture distribution qualitatively.

Moreover, previous studies indicated that tectonic stress differences affect the location and degree of fracture development—the closer to the fault, the greater the structural curvature and the more developed the fractures [15, 45-46]. This is true for the study area. Taking wells JL2010 and JL2004 as examples, the former is 1600 m away from the reservoir-controlling fault of the N–S boundary reservoir-controlling fault, with an average fracture density of 1.47 fractures/m and its dip angle is mainly lower than 60°, while the latter is 400-m away from the N–S boundary reservoir-controlling fault, with the average fracture density of 2.36 fractures/m and the fractures are mainly high angle fractures (mainly higher than 60°). Their fracture widths were also very different. This phenomenon reveals the influence of faults on the degree of fracture development. In addition, the structural burial depth also has a controlling effect on the fracture. The farther away from the fault, the greater the burial depth; the drilling-induced fracture is the main fracture development. The fracture development is relatively weak, such as JIN 216 and JIN220(see Fig.7g, Fig.7h). Thus, the structural position is the main controlling factor of fracture distribution (Table 3 and Fig. 4).

Additionally, even under the same tectonic stress background, the fracture development varies from lithology to lithology [42, 47-50]; see Fig. 6. The average fracture density of different volcanic rocks ranges from 1.3-2.7, but the fractures exhibit greater development in andesite (fracture density is 2.7) and basaltic breccia lavas (fracture density is 2.3). High-angle or vertical fractures developed in intermediate–acid volcanic lava and pyroclastic lava (e.g., andesite, rhyolite, andesitic volcanic breccia lava), while low-angle oblique fractures are found in irregular massive pyroclastic rocks. Reticular fractures formed by intersecting high-angle and low-angle oblique fractures are primarily observed in pyroclastic and intermediate lava (andesite), as seen in Fig. 7. In addition, under the same tectonic stress background, volcanic breccia lava and andesite are more prone to shear fracture owing to poor compression resistance (Tables 1 and 2).

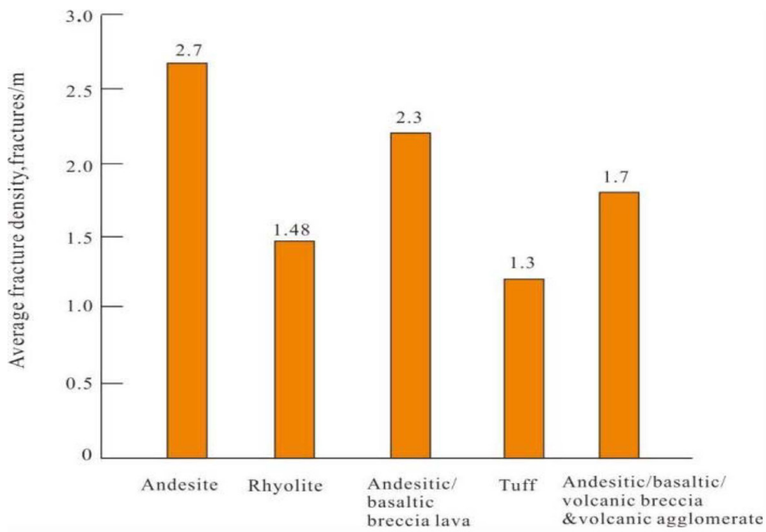

Fig. 6 Average fracture density by lithology of Jiamuhe Formation (P1j) volcanic rocks (core observation statistics data from 10 coring wells, the characteristics of fracture density distribution in different volcanic rocks. The fractures exhibit greater development in andesite and basaltic breccia lavas.)

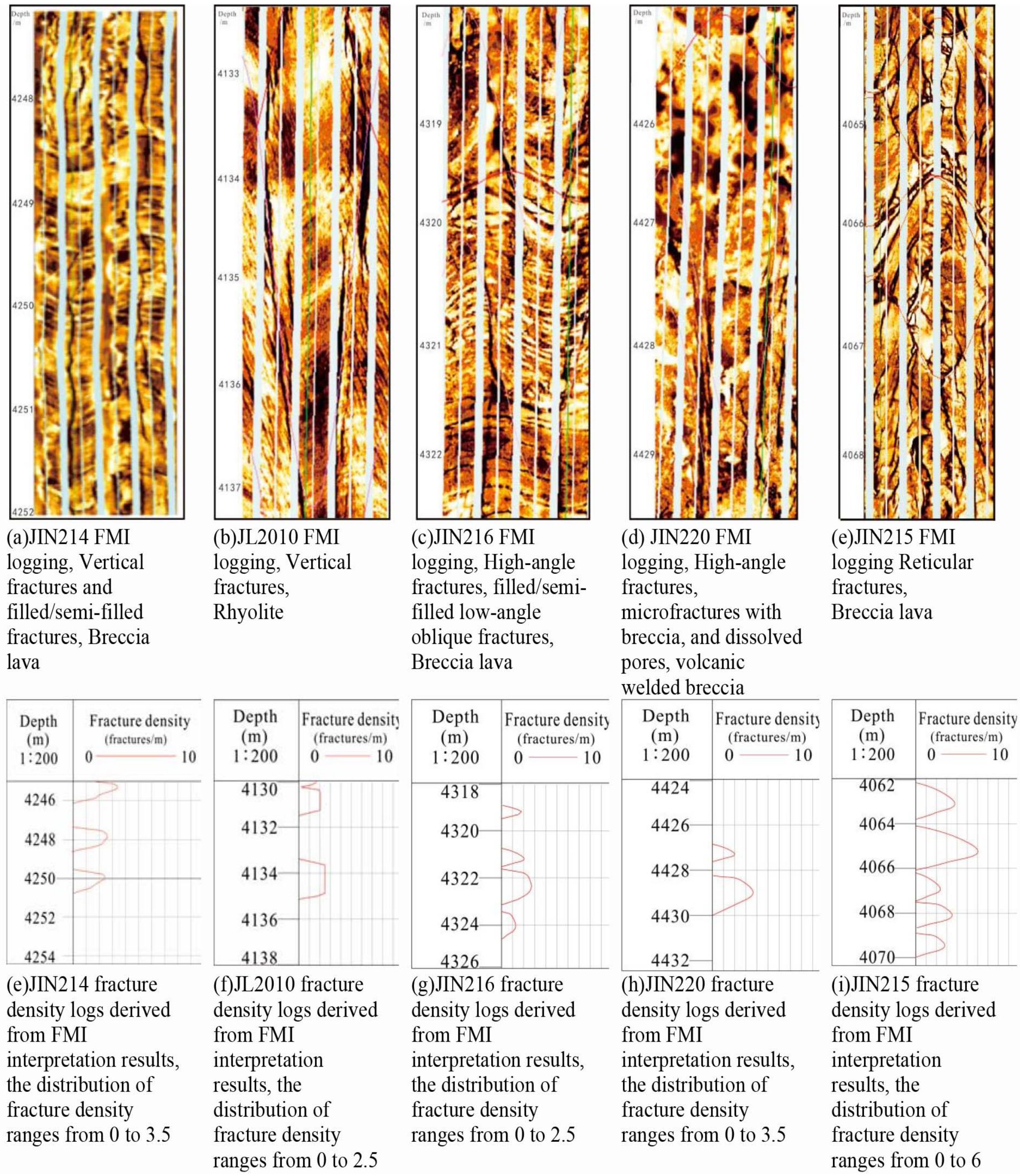

Fig. 7 Typical thriving imaging logging and fracture density logs derived from image logs in the volcanic reservoir of the Jiamuhe Formation (P1j).

Results and Discussion

Imaging Logging Identification and Description

Conventional logging data can only qualitatively identify fractures. To quantitatively describe the fractures in volcanic reservoirs and clarify the characteristics of fracture development to support the efficient development of the Jiamuhe Formation volcanic reservoir in the Jinlong 2 Oilfield, FMI (Formation MicroScanner Image) logging was conducted [32, 49, 51-52]. Moreover, the fracture types and their development in volcanic rocks with different lithologies are identified based on the FMI logging data. As shown in Fig. 7, the unfilled high-angle and vertical fractures are dark, low-resistivity stripes, mostly running from top to bottom of the core. In addition, the unfilled low-angle fractures exhibit dark, sinusoidal bedding. The semi-filled or filled high-angle, vertical, or low-angle fractures appear as white or bright stripes. The vesicles and dissolved pores or vugs appear as dark, low-resistivity spots. The volcanic breccia appears as bright spots. Based on fracture and lithology identification, the macroscopic fracture development is quantitatively described, involving density, length, width, dip angle, and porosity. Moreover, the FMI results show that the Jiamuhe Formation volcanic reservoir fractures display relatively large dip angles, mainly high-angle, vertical, and low-angle oblique fractures. In addition, the average fracture density is 1.47–3.02 fractures/m, the fracture width is 0.01–0.10 mm, and the fracture porosity is relatively small, with an average of 0.01%–0.15% (Table 3).

Prediction of Fracture Distribution by Prestack Seismic Inversion

The existence of fractures often leads to azimuthal anisotropy of underground media, which changes the seismic attributes (e.g., amplitude, frequency, attenuation). Moreover, the seismic wave amplitude anisotropy intensity is directly proportional to the fracture density. The more developed the fractures, the more anisotropic the amplitude variation with the azimuth. Prestack seismic data retain relatively more offset and azimuth information, ensuring the prediction of azimuthal anisotropy; therefore, they can describe the fracture density more reliably and accurately. Furthermore, the seismic wave azimuthal anisotropy characteristics can be extracted from the prestack seismic data, and then the fracture orientation and development intensity are analyzed according to the variation of seismic attributes with azimuth (Fig. 8). This approach is called amplitude versus azimuth or AVAZ [17, 24]. As per the P-wave reflection theory, the P-wave reflection coefficient changes with the incidence angle as an ellipse for a large fixed incidence angle. In addition, the oblateness of the ellipse indicates the fracture density, the long axis of the ellipse indicates the fracture orientation and the short axis of the ellipse indicates the fracture's normal direction. Accordingly, the responses of various seismic attributes that change with azimuth are extracted from the prestack seismic data containing the azimuth information. In addition, vertical or high-angle fractures in rocks can be detected by calculating the anisotropic ellipse.

In this study, referring to the Hudson fracture theory model [53], the prestack common middle point (CMP) gathered data of Jinlong 2 Oilfield were treated using AVAZ and prestack processing (including amplitude, frequency, attenuation) after the fidelity and amplitude preserving processing of the 3D seismic data. Then, the stack migration processing and attribute calculation were carried out for different azimuth data volumes. The anisotropy intensity and indicative fracture development degree of different amplitude dynamic attributes (e.g., prestack maximum energy, relative wave impedance, attenuation initial frequency) are compared. Moreover, compared with the fracture density interpreted by FMI logging data, the fracture density volume calculated using the single-well-attenuation initial frequency (the frequency value when the seismic amplitude is attenuated to 85%) is closer to the actual interpretation result (0.3), indicating a high coincidence rate up to 80% (Fig. 9). Thus, the attenuation initial frequency attribute is selected to simulate and calculate the Jiamuhe Formation fracture azimuth ellipse in the study area. The short axis direction of the azimuth ellipse indicates the statistical orientation (normal direction) of the fracture in space. In addition the ratio of the long to short axis is the flatness, which indicates the anisotropic strength of the seismic reflection and can indicate the fracture density so that the fracture density and orientation can be predicted. Moreover, the maximum principal stress derived from the core analysis and the fracture orientation interpreted by FMI logging data are both oriented nearly east-west, which is consistent with the fracture orientation predicted by AVAZ (Fig. 10). Furthermore, this proves that the prediction of fracture distribution by AVAZ in the Jiamuhe Formation of the Jinlong 2 Oilfield is reliable.

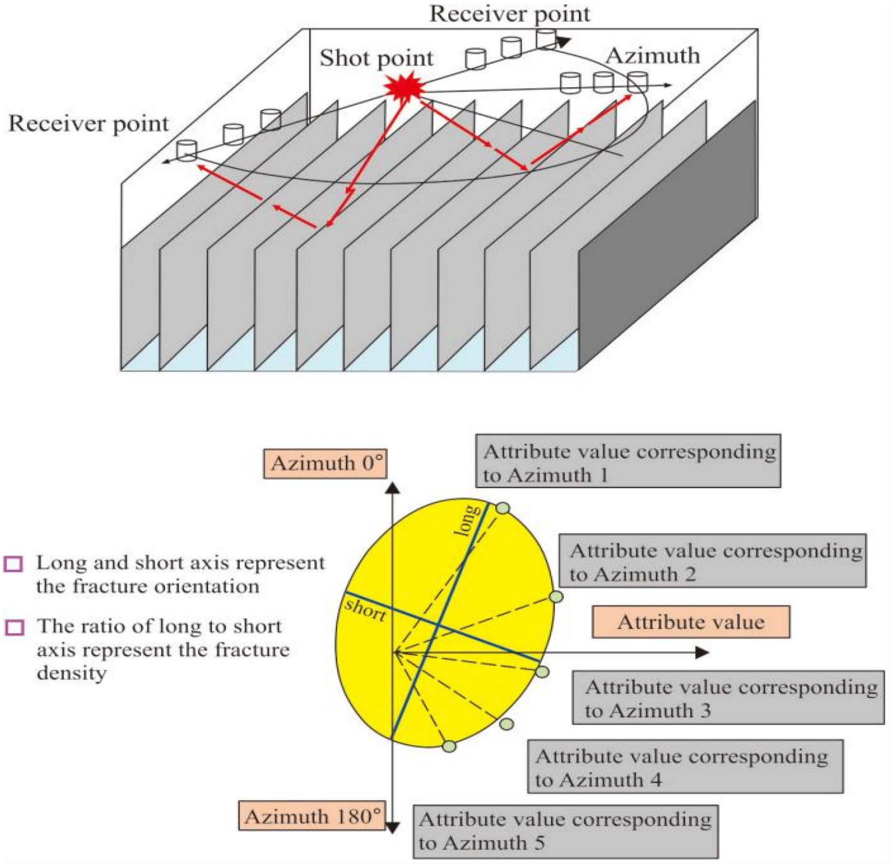

Fig. 8 Amplitude versus azimuth (AVAZ) schematic diagram.

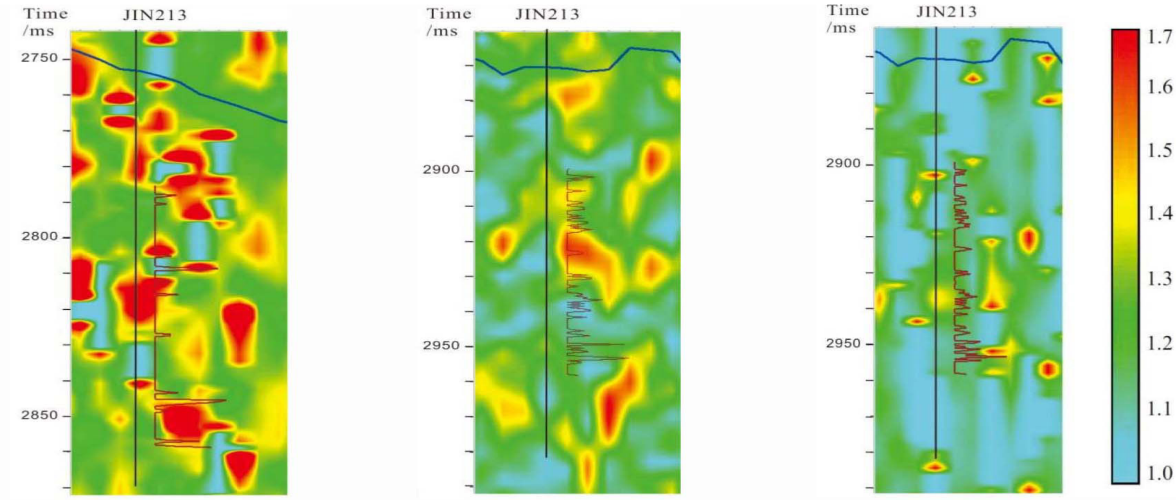

(a) Attenuation starting frequency (b) Relative wave impedance (c) Maximum prestack energy

Fig. 9 Prediction of fracture density by prestack seismic inversion (multiattribute comparison).

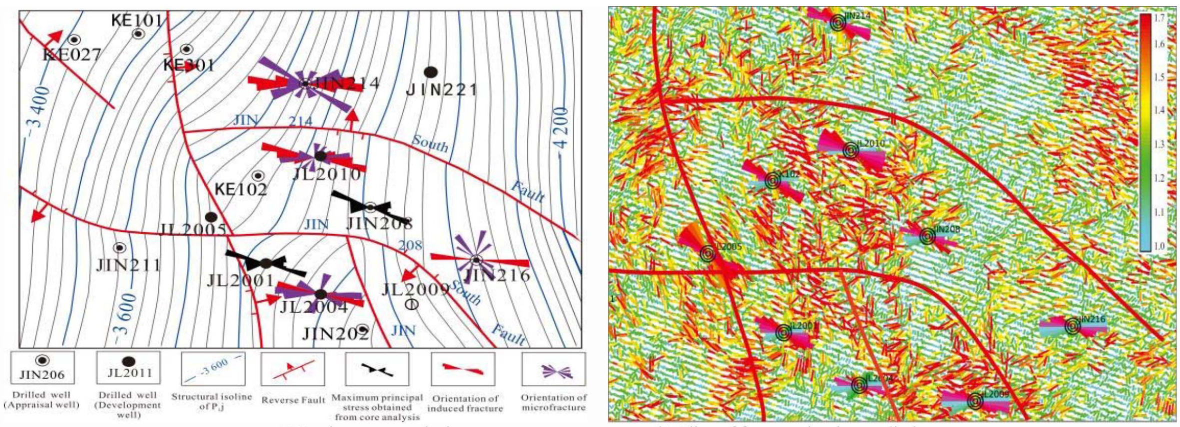

(a) In situ stress analysis (b) Slice of fracture density prediction

Fig. 10 Predicted fracture azimuth and in situ stress of the fault block in well JIN208 in the Jiamuhe Formation (P1j).

As per the predicted distribution of fractures in the entire study area (Fig. 11), controlled by both NW–SE and E–W faults, the fractures are well developed in the Jiamuhe Formation volcanic reservoir, and the closer to the fault, the more developed the fractures are. Moreover, at the axial intersections of fault blocks, the greater the structural deformation, the higher the degree of fracture development. This can be seen in the fault blocks in wells JIN208, JIN202, and JIN209. The study area is structurally high and steep in the north and low and gentle in the south. In addition, fractures are more developed in the north than in the south. According to slice-based fracture prediction, the development of fractures is weaker on horizons that are farther from the unconformity surface at the top of the Jiamuhe Formation. The farther away from the fault is, the greater the burial depth is, and the weaker the fracture developed, see Fig. 11a, Fig. 11b. Typical examples are the fault blocks in wells JIN214 and JIN201. In the areas with high fracture development and good matching between open fracture orientation and in situ stress direction, good results are obtained in single-well oil and production tests. Moreover, for example, in JL2010, where the fracture orientation is almost parallel to this maximum principal stress direction, the oil test at 4158–4189 m revealed a daily production of 15.34kg oil and 1760 m^3 gas with a 3-mm nozzle. The later 51 kg production test showed a cumulative oil production of 592.2 kg, gas production of 3.3 × 104 m3, and water production of 46.4kg, with an average daily oil production of 11.6 kg. In JIN212, the fracture orientation forms a large angle (>30°) with the present maximum principal stress direction, and primarily low-angle oblique fractures are developed locally, with few open fractures. As per the FMI interpretation, the daily oil production was 0.6 kg, and the water production was 3.6kg after perforation; after fracturing stimulation, the daily oil production with a 3-mm nozzle was 14.5 kg. Fractures are effective only when the dominant fracture orientation is consistent with or forms a small angle with this maximum principal stress direction; in such a case, the reservoir can have a high yield.

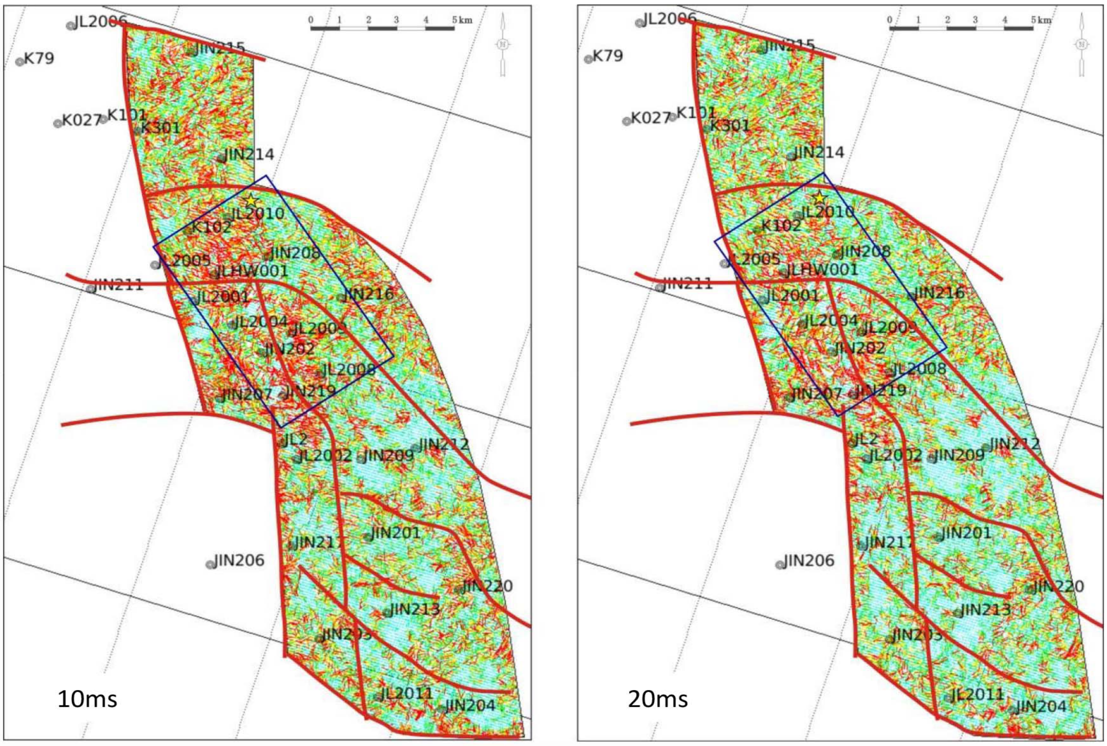

(a) 10 m from the top of the Jiamuhe (P_1j) Formation (15 m from the top)

(b) 20 m from the top of the Jiamuhe (P_1j) Formation (30 m from the top)

Fig. 11 Predicted fracture distribution in the Jiamuhe Formation (P1j) in the Jinlong 2 Oilfield

Conclusions

According to the studies which have been carried out, the following results are obtained:

1-The Jiamuhe Formation volcanic reservoir in the Jinlong 2 Oilfield has a variety of lithology, and reservoir characteristics are mainly controlled by lithology and lithofacies. High-angle, vertical, and low-angle oblique fractures are developed in the favorable reservoir intervals in the study area. These fractures are mostly unfilled or semi-filled and trend nearly east-west, which is approximately parallel to the direction of this maximum principal in situ stress, ensuring the opening of the fractures.

2-The complex fracture characteristics in the study area are affected by two main factors: structure and volcanic rock lithology. The structural fractures develop closer to the fault. The greater the structural deformation, the higher the degree of fracture development. The farther away from the fault, the greater the burial depth. The drilling-induced fracture is the main fracture development, and it is relatively weak.

3-The fracture development degree varies among volcanic rocks with different lithologies. High-angle or vertical fractures are primarily developed in intermediate to intermediate–acid volcanic and pyroclastic lava, such as andesite, dacite, and andesitic volcanic breccia lava. Low-angle oblique fractures are mainly developed in irregular, massive pyroclastic rocks, such as volcanic breccia and volcanic breccia lava. Reticular fractures formed by intersecting high-angle fractures and low-angle oblique fractures are mostly found in pyroclastic lavas and some intermediate lavas.

4-Considering that high-angle fractures dominate the study area, AVAZ is used to quantitatively predict the spatial distribution of fractures based on the single-well FMI logging interpretation results. The prediction results are compared with single-well FMI logging interpretation results, proving that AVAZ can improve prestack fracture prediction reliability. When the fracture development degree is high, and the open fracture orientation is consistent with or forms a small angle with the maximum principal stress direction, the single-well oil and production tests have good results. Fracture prediction by prestack seismic inversion provides an important reference for deploying development wells in the study area.

5-High fracture development and good matching between open fracture orientation and in situ stress direction, good results are obtained in single-well oil and production tests. The fractures are effective only when the dominant fracture orientation is consistent with or forms a small angle with this maximum principal stress direction, and the reservoir can have a high yield.

References

1. Cas, R., & Wright, J. (2012). Volcanic successions modern and ancient: A geological approach to processes, products and successions. Springer Science & Business Media. ISBN 978-0-412-44640-5.
2. Dai Shihua, L. X., Jun, W., & Shuyun, J. (1998). Log response and interpretation of velcanic rock reservoir. Xinjiang Petroleum Geology, 19(6): 465.
3. Gao, Q. T., Huang, S. Z., & Shi, X. Q. (1998). Study of conglomerate & volcanic rock reservoir using FMI log data. Well Logging Technology (in Chinese), 22, 55-59.
4. Li, C., Huang, L., Chen, L., & Yu, C. (2013, July). Bgg: A graph grammar approach for software architecture verification and reconfiguration. In 2013 Seventh International Conference on Innovative Mobile and Internet Services in Ubiquitous Computing, 291-298,

IEEE. doi: 10.1109/IMIS.2013.56.
5. Chen, G. H., & Fan, Y. R. (2000). An evaluation technique for volcanic reservoir using well-logging data. China Offshore Oil and Gas (Geology)(in Chinese), 14(6), 422-428.
6. Guo, Z. H., Wang, P. J., Yin, H., & Huang, L. (2006). Relationship between lithofacies and logging facies of the volcanic reservoir rocks in Songliao Basin. Journal of Jilin University(Earth Science Edition), 36(2): 207-214.
7. Young, E. L., & Paton-Walsh, C. (2010, August). Formaldehyde and nitrogen dioxide in smoke plumes from Australia's Black Saturday fires. In IOP Conference Series: Earth and Environmental Science, 11, No. 1, p. 012023). IOP Publishing. DOI: 10.1088/ 1755-1315/11/1/012023.
8. Xiao XL, Jin XJ, Zhang X, Liu H., Jiang Y (2015) Fracture identification based on information fusion of conventional logging and electrical imaging logging. Oil Geophysical Prospecting. 50(3): 542-547. DOI: 10.13810/j.cnki.issn.1000-7210.2015.03.023.
9. Wang, K., Yang, H. J., Zhang, H. L., Li, Y., Zhang, R. H., Yang, X. J. & Wang, J. P. (2018). Characteristics and effectiveness of structural fractures in ultra-deep tight sandstone reservoir: a case study of Keshen-8 gas pool in Kuqa Depression, Tarim Basin. Oil Geol. 39(4): 719-729. doi: 10.11743/ogg20180409.
10. Li, M., Zhou, F., Sun, Z., Dong, E., Zhuang, X., Yuan, L., & Wang, B. (2022). Experimental study on plugging performance and diverted fracture geometry during different temporary plugging and diverting fracturing in Jimusar shale. Journal of Petroleum Science and Engineering, 215, 110580. ISSN: 0920-4105.
11. Chen, G. H., Wu, W. S., & Wang, Z. W. (1999). Fracture identification by microresistivity scanner log. Well Logging Technology (in Chinese), 23(4): 279-281. doi: CNKI: SUN: CJJS.0.1999-04-011.
12. Nie, X., Zou, C., Pan, L., Huang, Z., & Liu, D. (2013). Fracture analysis and determination of in-situ stress direction from resistivity and acoustic image logs and core data in the Wenchuan Earthquake Fault Scientific Drilling Borehole-2 (50–1370 m). Tectonophysics, 593, 161-171, doi.org/10.1016/j.tecto.2013.03.005.
13. Deng, P. (2002). Log response and explanation of structural fractures in volcanic rock reservoir. Acta Petrolei Sinica, 23(6): 32. doi: 10.3321/ j.issn: 0253-2697. 2002.06.007.
14. Chen, Y., & Tan, M. J. (2003). Fracture detection and identification using logging techniques. Well Logging Technology (in Chinese), 27(S1): 11-14.
15. Zhou, X. G., Cao, C. J. & Yuan, J. Y. (2003). The research actuality and major progresses on the quantitative forecast of reservoir fractures and hydrocarbon migration law, Advance in Earth sciences. 18(3): 400- 403. doi: 10.11867/j.issn.1001-8166.2003.03.0398.
16. Chen, J. L., Lan, S. Q. & Wang, C. J. (2004). Prediction of Fractured Reservoirs Using Seismic Technology and Its YANG, G. F., Gang, W. A. N. G., GAO, J. S., & XU, C. M. (2007). Coke formation and olefins conversion in FCC naphthaolefin reformulation at low reaction temperature. Journal of Fuel Chemistry and Technology, 35(5): 572-577. doi: 10.1016/S1872-5813(07)60034-6.
17. Guo-hua, Z. H. U., Yi-qin, J. I. A. N. G., & Xian-jing, L. I. (2008). The volcanic reservoir characteristics of Jamuhe Formation in Zhongguai-District 5-(8) area in Karamay oilfield. Xinjiang Petroleum Geology, 29(4): 445. doi: JournalArticle/ 5aed40dac095d710d409f7a6.
18. Sun, Z. C., Jiang, Y. Q., Ming, Z., Chen, Z. H., Chang, Q. S., & Chun-Li, X. U. (2013). Lithology-lithofacies model of Carboniferous volcanic reservoirs in the Junggar Basin, NW China. Journal of China University of Mining & Technology, 42(5), 782-789.
19. Dong, G.D., Zhang, Q., Zhu, X. M., Xian, B. Z., Zhu, S. F., Niu, H. P. & Chen, Q. Y. (2014). Current status and problems of volcanic reservoir study: an example from the Lower Permian volcanic rocks in Ke-Xia area of Junggar Basin. Oil & Gas Geology (in Chinese). 33(4): 511-519. doi: 10.11743/ogg20120403.
20. Guo-ping, L. I. U., Lian-bo, Z. E. N. G., Mao-sheng, L. E. I., Ke-wei, Z. U., Fei, W., & Qi, L. (2016). Fracture development characteristics and main controlling factors of the volcanic reservoir in Xujiaweizi fault depression. Geology in China, 43(1), 329-337.
21. Lu, Y., Lü, H., Cui, Y., & Chen, H. (2018). Method for fracture effectiveness evaluation based on 3D Mohr Circle and its application. Acta Petrolei Sinica, 39(5): 564. doi: 10.7623/syxb201805007.
22. Cao, Y. M., Zhang, C. G., Yang, W. Y. & Xu, J. L. (2006). Fractured reservoir porosity quantitative evaluation using electric imaging logging data. Well Logging Technology (in Chinese). 30(3): 237-239. doi:10.1016/ S1001-8042(06)60011-0.
23. QiGang, G. (2005). Application of AVA fracture detection technique. Natural Gas Industry, 25(5): 42.
24. Chen, D., Chen, L. Q., Wei, X. C. & Wang, Z. (2011). Log evaluation of fractured igneous reservoirs: A case study of the Carboniferous igneous reservoirs in the Junggar Basin. Oil & Gas Geology (in Chinese). 32(1): 83-90. doi: 10.1007/s12182-011-0123-3.
25. Song, M. S., He, N. Q., Yang, S. C., Zhao,Y. F. & Niu, H. R. (2017). Study on the fracture distribution pattern of volcanic rock in thrust fault developed zone. Natural Gas Geoscience. 28(7): 989-999. doi: 10.11764/j.issn. 1672-1926.2017.06.011.
26. Hai-rui, N., Shao-chun, Y., Yong, W., Ni-qian, H., & Bao-quan, M. (2017). Analysis on the formation periods of fractures of volcanic reservoirs in Chepaizi area, Junggar Basin. Natural Gas Geoscience, 28(1): doi: 10.11764/j.issn. 1672-1926.2016.11.021.
27. Ibrahim, A. F., Ibrahim, M., Sinkey, M., Johnston, T., & Johnson, W. (2020, October). Evaluation of single fracture stage performance with integrated rock mechanics and pressure transient analysis. In SPE Annual Technical Conference and Exhibition?, (p. D031S033R006). SPE, doi.org/10.2118/201638-MS.
28. Fu, J. W., Xiao, L. Z. & Zhang, Y. Z. (2004). Status and developing trend of acoustical and electrical imaging well logging tools. progress in geophysics. 19(4): 730-738. doi: 10.1016/S0960-0779(03) 00420-X.
29. Jia, C. M., Zhi, D. M., & Xing, C. Z. (2009). Features and control factors of volcanic rock reservoir in the

Chepaizi uplift, Junggar basin. Acta Geologica Sinica (in Chinese), 29(1), 33-36. doi: 10.3969/j.issn. 1006-0995.2009.01.009.

30. He, S., Yang, S., Shao, X., & Shi, A. (2011). Ship target detection on the sea surface based on natural measure feature of image block. Infrared and Laser Engineering, 40(9). doi: CNKI: SUN: GWCJ. 0.2011-02-026.
31. Zhang, Y., & Pan, B. Z. (2012). On three calculation methods of volcanic reservoir fracture porosity based on FMI data. Well Logging Technology, 36(4): 365-369.
32. He, H., Li, S., Liu, C., Kong, C., Jiang, Q., & Chang, T. (2020). Characteristics and quantitative evaluation of volcanic effective reservoirs: A case study from Junggar Basin, China. Journal of Petroleum Science and Engineering, 195, 107723, doi.org/10.1016/j.petrol.2020.107723.
33. Zhang, L. & Zhou, Y. S. (2004). Evaluation criteria for development degree of micro cracks in oil and gas reservoir. Acta Petrolei Sinica. 25(4), 33-37. doi: 10.7623/syxb200404007.
34. He, Y. D. & Wei, C. G. (2007). The present situation and research direction of evaluation methods in fracture type reservoir. Progress in Geophysics (in Chinese). 22(2): 537-543. doi: 10.1007/ s11442-007-0020-2.
35. Tang, X. Y., Wang, X. Y., & Zhu, Y. H. (2009). Use synthetic probability method to evaluate the fracture development of volcanic rocks. Natural Gas Exploration and Development (in Chinese), 32(1): 26-27.
36. 37. Wang, C. Y., Gao, T. (2009). Identifying and evaluating the fractures by the Formation MicroImager (FMI) log and estimating parameters of fractures: A case study of Xushen gas field. Natural Gas Industry (in Chinese). 29(8): 38-41. doi: 10.1287/mksc.1080.0385.
37. ZHAO, H., SHI, X., & Li-qiang, S. (2012). Study on porosity exponent, saturation and fracture porosity for fractured reservoirs. Progress in Geophysics, 27(6): 2639-2645, doi: 10.6038/j.issn.1004-2903.2012.06.043.
38. Chen, S. M., Jiang, C. J., Liu, L., Chu, L. L. & Pei, M. B. (2014). Fracture formation mechanism of volcanic rocks in Xujiaweizi fault depression of Songliao Basin. Journal of Jilin University (Earth Science Edition). 44(6): 1816-1826. doi: 10.13278/j.cnki.jjuese.201406110.
39. Haizhou, Q. U., Zhang, F., Zhenyu, W. A. N. G., Xiangtong, Y. A. N. G., Hongtao, L. I. U., Dan, B. A., & Xi, W. A. N. G. (2016). Quantitative fracture evaluation method based on core-image logging: A case study of Cretaceous Bashijiqike Formation in ks2 well area, Kuqa depression, Tarim Basin, NW China. Petroleum Exploration and Development, 43(3), 465-473. doi: 10.1016/S1876-3804(16)30054-4.
40. Yang, S. C., Niu, H. R., Song, M. S., Zhao, Y. F. & Wang, Y. (2017). Quantitative characterization of development degree of fault-related fracture in compressional thrust structure block of the Carboniferous in Chepaizi area. Journal of China University of Petroleum. 41(5):1-8. doi: 10.3969/ j.issn.1673-5005.2017.05.001.
41. Lu, Z., Tao, M., Zhen-hong, W., Wen-hui, Z., Jiang-wei, S., Wei-li, C., Mei, L. and Qi, Z. (2017). Classification and combination characteristics of fractures in super-deep tight sandstone reservoir of Keshen Gasfield in Tarim Basin. Natural Gas Geoscience, 28(11). doi: 10.11764 / j. issn. 1672G1926. 2017. 09. 010.
42. ZHANG, H., Guoqing, Y., & Haiying, W. A. N. G. (2019). Effects of natural fractures geomechanical response on gas well productivity in Kuqa Depression, Tarim Basin. Natural Gas Geoscience, 30(3): 379-388. doi: 10.11764/j.issn. 1672-1926.2018.10.020.
43. Ju, W., You, Y., Feng, S. B., Xu, H., Zhang, X., & Wang, S. (2020). Characteristics and genesis of bedding-parallel fractures in tight sandstone reservoirs of Chang 7 oil layer, Ordos Basin. Oil Gas Geol, 41(03): 596-605. doi: CNKI: SUN: SYYT.0.2020-03-016.
44. Liu, J. H., Yang, S. C., Chen, N. N. & Zhao, X.D. (2009). Forecasting method of tectoclase in the igneous reservoirs using a curvature of the microtetctonics. Journal of China University of Mining & Technology. 38(6): 815-819.
45. Sun, W., Li, Y. F., Fu, J. W. & Li, T. Y. (2014). Review of fracture identification with well logs and seismic data. Progress in Geophysics (in Chinese). 29(3): 1231-1242. doi: 10.6038/pg20140332.
46. Lu, S. K., Wang, D., Li, Y. K., Meng, X. J., Hu, X. Y. & Chen, S. W. (2015). Research on three-dimensional mechanical parameters'distribution of the tight sandstone reservoirs in Daniudi Gasfield. Nat. Gas Geosci. 26, 1844-1850. doi: 10.11764/j.issn.1672-1926.2015.10.1844.
47. Sun, H., Zhong, D., & Zhan, W. (2019). Reservoir characteristics in the Cretaceous volcanic rocks of Songliao Basin, China: A case of dynamics and evolution of the volcano-porosity and diagenesis. Energy Exploration & Exploitation, 37(2): 607-625. doi: 10.1177/0144598718812546.
48. Wang, Z., Jin, L. X., Guan, Q., Yang, L., & Wu, J. L. (2010). Comprehensive evaluation of volcanic reservoir based on FMI and ECS. Journal of Southwest Petroleum University(Science & Technology Edition), 32(5): 58-64.
49. Yarmohammadi, S., Kadkhodaie, A., & Hosseinzadeh, S. (2020). An integrated approach for heterogeneity analysis of carbonate reservoirs by using image log based porosity distributions, NMR T2 curves, velocity deviation log and petrographic studies: A case study from the South Pars gas field, Persian Gulf Basin. Journal of Petroleum Science and Engineering, 192, 107283. doi: 10.1016/j.petrol.2020.107283.
50. Wu, H., Zhang, X., Li, X., Liao, P., Li, W., Li, Z., Wu, Y. and Pei, F. (2006). Studies on acute toxicity of model toxins by proton magnetic resonance spectroscopy of urine combined with two-step cluster analysis. Chinese Journal of Analytical Chemistry, 34(1): 21-25. doi: 10.1016/S1872-2040(06)60004-2.
51. Xiang, M., Qin, P. B., Zhang, F. W. (2020), Research and application of logging lithology identification for igneous reservoirs based on deep learning, Journal of Applied Geophysics, 173. doi: 10.1016/j.jappgeo.2019.103929.
52. Hudson, J. A. (1981). Wave speeds and attenuation of elastic waves in material containing cracks. Geophysical Journal International, 64(1), 133-150. doi: 10.1111/j.1365-246X.1981. tb02662.x.